Anti-Windup Design for Fixed-Tilt Hexarotor in Aerial Physical Interaction

Dharani Jayanna[1], Davide Invernizzi[1], Daniele Migliore[2], Simone Panza[2], Marco Lovera[1]

***Abstract*— This paper presents an anti-windup (AW) augmentation scheme designed to recover the performance of an unconstrained baseline controller under actuator saturation for a hexarotor with fixed-tilt propellers. The fixed-tilt configuration, which enhances the maneuverability and interaction capabilities compared to standard coplanar systems, also introduces direction-dependent force limits that must be carefully addressed in the design of control laws. Our method integrates the linearized dynamics of the hexarotor with its mixer matrix and synthesizes the AW compensator via LMI-based optimization. Simulation results show that, under actuator saturation conditions, the AW-augmented controller closely matches the unconstrained controller's behavior while reducing transient dynamics and altitude loss due to external disturbances. These results underscore the potential of the proposed framework for enhancing UAV performance during complex maneuvers particularly during aerial interaction.**

I. Introduction

In the past decade, the field of aerial robotics has seen significant advancements with the development of fully actuated unmanned aerial vehicles (UAVs), which offer enhanced capabilities compared to conventional underactuated systems. These UAVs utilize non-coplanar propeller configurations to enable independent control of both translational and rotational dynamics, greatly improving their ability to interact with the environment. This advancement has proven valuable in applications such as aerial manipulation [1] and contact-based aerial inspection [2]. While full actuation is typically achieved through active tiltrotor designs with servo-actuated propellers, some systems adopt fixed propeller orientations to meet specific force and torque requirements, resulting in UAVs with full or partial actuation capabilities. Fixed-tilt designs are favored for their mechanical simplicity and fewer design parameters, and often feature a simpler design of control system but they come with the limitations in generating forces along the lateral and longitudinal axes. These limitations, which are a function of the cant and dihedral angles of the propellers, restrict the UAV's ability to perform a wide range of full-pose trajectories, especially during steady hovering or under external disturbances such as wind gusts.

Despite efforts to optimize the cant and dihedral angles for improved control wrench and flying efficiency, the limited lateral and longitudinal force generation remains a significant constraint in fixed-tilt UAVs, particularly for platforms used in aerial interaction tasks. In these applications, where specific force directions are often required for effective manipulation or interaction with the environment, the fixed-tilt configuration introduces a critical challenge. The tilting and arrangement of the propellers must be carefully balanced to achieve optimal force generation while considering trade-offs, such as mechanical feasibility, maneuverability, and stability. This limitation can lead to actuator saturation, where the system reaches the maximum available force and torque, compromising both performance and stability. Actuator saturation is a well-known nonlinear phenomenon in control systems, and numerous methods have been proposed to address it, including model predictive control [3], sliding mode control [4], and others. Among these, the design of an anti-windup (AW) compensator has proven to be one of the most effective strategies, providing stability and performance guarantees in the presence of saturation [5]. Our research builds on this approach, focusing on the design of an AW compensator for a fixed-tilt hexarotor that tracks full-pose trajectories sensitive to lateral force constraints, which often lead to actuator saturation.

In our previous works, we addressed actuator saturation in quadrotors, focusing on attitude control that induces integral windup effects [6], as well as directionality issues in position and yaw control [7]. However, the design of an AW compensator for fully actuated UAVs is presented for the first time in this work. The proposed AW compensator utilizes a generalized sector condition [8] to model the saturation nonlinearity and minimizes the performance degradation caused by saturation. We formulate the AW design as a Linear Matrix Inequality (LMI) optimization problem [9], prioritizing control objectives and time-domain performance under practical conditions. To replicate the reference signals of interest, the AW synthesis model incorporates a filter. The performance of the augmented controller was evaluated through simulations of a lateral plane maneuver in the fixed-tilt hexarotor, where steady attitude during hover leads to saturation of lateral force constraints and loss of positional stability. Simulation results demonstrated that the proposed AW compensator improves performance during such maneuvers and effectively prevents harmful or undesirable motions caused by actuator saturation.

Notation: In this paper $\mathbb{Z}(\mathbb{Z}_{>0},\mathbb{Z}_{\geq 0})$ denotes the set of integers (positive, non-negative integers), $\mathbb{R}(\mathbb{R}_{>0},\mathbb{R}_{\geq 0})$ denotes the set of real numbers (positive, non-negative real numbers), $\mathbb{R}^n$ denotes the n-dimensional Euclidean space and $\mathbb{R}^{m\times n}$ the set of $m\times n$ real matrices. The i th vector of the canonical basis of $\mathbb{R}^n$ is denoted as e_i and the identity matrix in $\mathbb{R}^{n\times n}$ is denoted as $I_n=[e_1\cdots e_i\cdots e_n]$. Given $A\in\mathbb{R}^{n\times n}$, we use the compact notation $A\in\mathbb{R}^{n\times n}_{>0}\left(\mathbb{R}^{n\times n}_{<0}\right)$ to represent a positive (negative) definite matrix. For a square matrix X, we denote $\mathrm{He}(X)=X+X^\top$. Given a sequence $x(t), t\in\mathbb{Z}_{\geq 0}, x^+$ is a shorthand notation for $x(t+1)$. Function sat $u^{\bar{u}}_{\underline{u}}(\cdot)$ denotes the decentralized saturation function, i.e., given $u\in\mathbb{R}^n$

[1]Dharani Jayanna, Davide Invernizzi and Marco Lovera are with Dipartimento di Scienze e Tecnologie Aerospaziali, Politecnico di Milano, Via La Masa 34, 20156 Milano, Italy. email: dharani.jayanna@polimi.it.

[2]Daniele Migliore and Simone Panza are ANT-X s.r.l., via Davanzati 33, 20158 Milano, Italy. email: simone@antx.it.

and some bounds $\underline{u}, \bar{u} \in \mathbb{R}^n_{>0}$, $\text{sat}^{\bar{u}}_{\underline{u}}(u) = (\max(\min(\bar{u}_1, u_1), -\underline{u}_1), \ldots, \max(\min(\bar{u}_n, u_n), -\underline{u}_n))$. Finally, $\overline{\text{co}}\{v_r \in \mathbb{R}^n, r = 1, \ldots, n_v\}$ is the closed convex hull, i.e., the smallest closed convex set that contains the points identified by the vectors v_r. The map $S(\cdot) : \mathbb{R}^3 \to \text{SO}(3) = \{W \in \mathbb{R}^{3\times 3} : W = -W^\top\}$ is defined such that given $a, b \in \mathbb{R}^3$ one has $S(a)b = a \times b$.

II. Background and Problem Statement

In this work, we consider a multirotor named ARIES [10], developed by ANT-X for contact-based aerial inspection in non-destructive testing (NDT) applications. The platform features a non-conventional fixed-tilt configuration, similar to [11], with six rotors symmetrically arranged along the longitudinal axis. The rotors are tilted at predefined angles as shown in Figure 1 to enable the UAV to generate an overall thrust component within the plane of the central body, in addition to the vertical out-of-plane component. The motion

Fig. 1. ARIES fixed-tilt hexarotor.

of the UAV is described by referring to a body-fixed frame $F_B = (O_B, \{b_1, b_2, b_3\})$ located at the center of mass with respect to a reference frame $F_I = (O_I, \{i_1, i_2, i_3\})$, where b_j and i_j for $j \in \{1, 2, 3\}$ are unit vectors forming right-handed orthogonal triads and O_B, O_I are the origins of the body and reference frame, respectively. In the following, the position vector from O_I to O_B, resolved in F_I, is denoted as $x \in \mathbb{R}^3$ while the rotation matrix describing the orientation of the UAV is denoted as $R = \begin{bmatrix} b_1 & b_2 & b_3 \end{bmatrix} \in \text{SO}(3)$, where b_i is the i-th body axis resolved in F_B. The equations for translational and rotational dynamics can be expressed as

$$\begin{aligned} \dot{x} &= v, & m\dot{v} &= -mge_3 + Rf_c, \\ \dot{R} &= RS(\omega), & J\dot{\omega} &= -S(\omega)J\omega + \tau_c, \end{aligned} \tag{1}$$

where $J = J^\top \in \mathbb{R}^{3\times 3}_{>0}$ is the UAV inertia matrix with respect to O_B, $m \in \mathbb{R}_{>0}$ is the UAV mass, $g = 9.81\ \text{m/s}^2$ is the gravitational acceleration, $\omega \in \mathbb{R}^3$ is the body angular velocity, $v \in \mathbb{R}^3$ is the inertial translational velocity. The control wrench is given by $w_c = \begin{bmatrix} f_c^\top & \tau_c^\top \end{bmatrix}^\top \in \mathbb{R}^3 \times \mathbb{R}^3$.

Various control methods have been studied [12] for tracking a fully independent six-DOF trajectory for a given desired position x^d, velocity v^d (both in the inertial frame F_I), and attitude $R \in \text{SO}(3)$ and angular velocity ω^d (both in the body frame F_B). In this work, we employ a nonlinear cascaded controller for independent position and attitude regulation. Specifically, the control architecture consists of a double cascade of P/PD controllers for position and attitude control, computing the desired control wrench as

$$\begin{aligned} f_c &= m\left(K_{(P,v)}R^\top\left(K_{(P,x)}e_x + e_v\right) - D_v(z)v\right) + R^\top mge_3, \\ \tau_c &= K_{(P,\omega)}\left(K_{(P,\Theta)}e_\Theta + e_\omega\right) - D_\omega(z)\omega, \end{aligned} \tag{2}$$

where $K_{(P,(\cdot))} \in \mathbb{R}^{3\times 3}_{>0}$ is a diagonal gain matrix while e_x, e_v, e_Θ, and e_ω are the error vectors in $\mathbb{R}^3$ defined as $x^d - x$, $v^d - v$, $\Theta^d - \Theta$, and $\omega^d - \omega$ respectively such that the attitude representing roll, pitch, and yaw angles in body frame F_B is given by $\Theta = [\phi\ \theta\ \psi]^\top$. The function $D_{(\cdot)}(z)$ is given by $K_{D,(\cdot)}N_{(\cdot)}\frac{z-1}{z-1+N_{(\cdot)}T_s}I_3$ such that it is a discrete transfer function diagonal matrix describing derivative action. $T_s \in \mathbb{R}_{>0}$ denotes the sampling time, $K_{D,(\cdot)} \in \mathbb{R}^{3\times 3}_{>0}$, and $N_{(\cdot)} \in \mathbb{R}_{>0}$ are the diagonal matrices containing the derivative gains and filter time constants respectively.

The controller computes the desired forces and moments in the UAV body frame F_B, which must be mapped onto the propeller forces across the six rotors. Since the propeller planes are tilted, this transformation requires careful consideration of their orientations. To achieve this, we define six reference frames F_{R_i} for $i = \{1, \ldots, 6\}$, where the origin O_{R_i} coincides with the center of rotation of the i-th propeller group. The orientation of each F_{R_i} relative to the body frame F_B is determined through a sequence of rotations. Starting from the body frame F_B, the transformation consists of a rotation about the z_b-axis of the body frame by an angle ψ_i, followed by a rotation about an intermediate y'-axis by an angle β_a. Next, the frame is rotated about an intermediate x''-axis by an angle α_i, and finally, a rotation is applied about an intermediate y'''-axis by an angle β_i. These sequential rotations define the orientation of each propeller frame F_{R_i} with respect to the body frame as given by

$$R^{R_i}_B = R_Y(\beta_i)R_X(\alpha_i)R_Y(\beta_a)R_Z(\psi_i), \tag{3}$$

such that $R^{R_i}_B = R^B_{R_i}{}^\top$. The sequence of tilting angles α_i and β_i follows the manufacturing process: first, the i-th rotor arm is tilted by α_i, and then the motor is adjusted by β_i about the y'''-axis. Additionally, an arm tilt angle β_a accounts for the rotation of the arms about the y'-axis relative to the $b_1 - b_2$ plane (i.e., the horizontal plane in the body frame). This feature accommodates mounting configurations such as folding mechanisms. The angle β_a is assumed to be the same for all arms.

Tilting the rotors around the axes coinciding with the vehicle arms (non-zero cant angles) significantly enhances maneuverability compared to tilting around axes perpendicular to the arms (non-zero dihedral angles) [13]. While dihedral angles improve stability and enable steady hovering, cant angles directly influence dynamic maneuverability, making them crucial for interaction tasks. The cant angles also affect the UAV's force and torque envelope, which is key for aerial interaction. By adjusting these angles, the UAV can generate the required forces and torques for tasks like manipulation or inspection. Proper cant angle selection ensures torque decoupling, gravity compensation, and effective interaction with the environment while maintaining stability.

Using equation (3), the control wrench induced by the

propulsive system is given by

$$\begin{aligned} f_c &= \sum_{i=1}^{6} \left(-f_i R^B_{R_i} e_3\right), \\ \tau_c &= \sum_{i=1}^{6} \left(-\mathrm{S}\left(x^B_{BR_i}\right) f_i R^B_{R_i} e_3 + (-1)^{i-1} k^\tau_f f_i R^B_{R_i} e_3\right), \end{aligned} \tag{4}$$

where $x^B_{BR_i}$ represents the position of each propeller center O_{R_i} expressed in F_B. Considering the transformation defined in equation (3), it can be rewritten as $x^B_{BR_i} = \left(R_Y(\beta_a) R_Z(\psi_i)\right)^\top \ell_i e_1$ where $\ell_i > 0$ is the length of the arm from O_B to the i-th rotor. The coefficient $k^\tau_f \in \mathbb{R}_{>0}$ is the ratio of torque to thrust coefficient determined experimentally and $f_i \in \mathbb{R}_{\geq 0}$ is the propulsive force of the i-th rotor such that

$$f_u = \begin{bmatrix} f_1 & f_2 & f_3 & f_4 & f_5 & f_6 \end{bmatrix}^\top \in \mathbb{R}^6_{\geq 0} \tag{5}$$

contains the propulsive force of all the rotors. The control wrench as defined in equation (4) can be expressed through the linear mapping

$$w_c = F f_u, \tag{6}$$

where $F \in \mathbb{R}^{6\times 6}$ is the *input* map. Matrix F is a nonlinear function of the tilting angles and its i-th column has the following form:

$$F_i := \begin{bmatrix} -R^B_{R_i} e_3 \\ \left(-\mathrm{S}(x^B_{BR_i}) + (-1)^{i-1} k^\tau_f I_3\right) R^B_{R_i} e_3 \end{bmatrix}. \tag{7}$$

III. Saturation Limits on the Desired Control Wrench

In the previous section, we defined the transformation from the propulsive forces of all six rotors to the forces and moments in the body frame F_B as given in equation (6). Provided that the propellers are suitably positioned and oriented within the airframe, the input matrix F in (6) is invertible by design. Then, the *mixer* mapping (or *allocation* mapping) is defined as the matrix that relates the forces and moments requested by the controller (w_c) to the thrust required from each propeller (f_i). This matrix is simply given by the inverse of the *input* matrix and allows allocating the control wrench according to:

$$f_u = F^{-1} w_c. \tag{8}$$

Propellers are inherently limited by their finite, unidirectional thrust-generating capacity, which acts normal to their rotational plane. This constraint can be expressed as

$$f^a_u = \mathrm{sat}^{\bar{u}}_{\underline{u}}(f_u), \tag{9}$$

where f^a_u denotes the applied propeller force on the rotors, with the minimum and maximum propulsive forces defined as $\underline{u}$ (which is zero) and $\bar{u}$, respectively. These limits directly constrain the forces and moments that can be generated in the body frame, as dictated by the *input* matrix. Moreover, because the rotors are tilted, the maximum achievable thrust varies with direction, resulting in non-uniform force limits. To accurately capture these direction-dependent constraints, we perform an iterative analysis to determine the feasible range of control forces and moments that each rotor can produce while adhering to its individual limits.

Figure 2 (left) shows the overall feasible control forces that can be generated along the longitudinal ($f_{c_{b_1}}$), lateral ($f_{c_{b_2}}$), and vertical ($f_{c_{b_3}}$) axes in the body frame F_B. This three-dimensional force envelope, which takes the form of an irregular hexahedron, is primarily shaped by the allocation matrix F. Since the fixed-tilt platform is designed to operate in a fully actuated mode during hovering, it is particularly important to consider the force limits in the b_1–b_2 plane. This scenario is represented by the horizontal cross-section of the hexahedron at a constant vertical force, $f_{c_{b_3}} = mg$. Figure 2 (right) presents this two-dimensional cross-section,

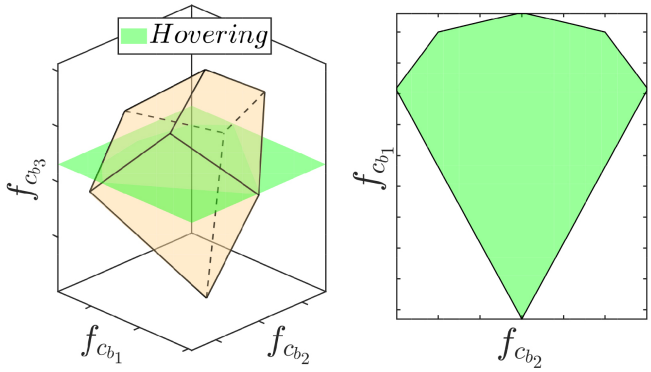

Fig. 2. Feasible force volume (on the left) and force limits (on the right) during hovering along the b_1-b_2 plane of the fixed-tilt hexarotor (scale not shown for confidentiality)

which exhibits a diamond shape with an elongated lower portion. This geometry indicates that the range of achievable lateral forces is very limited, while the force envelope mainly develops along the longitudinal direction. The typical control scheme protects against saturation by projecting the commanded force and torque within feasible regions, but it does not guarantee stability or performance. In contrast, our approach computes the desired forces and moments and addresses saturation with an AW augmentation, ensuring stability and robust performance.

IV. Anti-Windup Augmentation Strategy for Fixed-Tilt UAVs

In this section we recall the AW design proposed by [14], which is cast as an LMI-based optimization problem following the modern framework of the Direct Linear Anti-Windup (DLAW) design and leveraging the performance-oriented approach presented in [9]. To implement the proposed AW strategy, the fixed-tiltrotor model as described in equation ((1)) must be linearized. Assuming near hovering conditions at a given position $\left(\bar{x} \in \mathbb{R}^3\right)$, such that $x \approx \bar{x} + \Delta x$, $v \approx \Delta v$, $\omega \approx \Delta\omega$, $R \approx I_3 + S(\Delta\Theta)$ where $\Delta\Theta = \begin{bmatrix} \phi & \theta & \psi \end{bmatrix}^\top$ representing small rotation angles in roll, pitch and yaw respectively, the linearized dynamics is given by

$$\begin{aligned} \dot{\Delta x} &= \Delta v, \quad & \dot{\Delta\Theta} &= \Delta\omega, \\ J\dot{\Delta\omega} &= \Delta\tau_c, \quad & m\dot{\Delta v} &= -mgS(\Delta\Theta)\, e_3 + \Delta f_c, \end{aligned} \tag{10}$$

where Δf_c is equal to $f_c - mge_3$ and $\Delta\tau_c = \tau_c$ representing deviation variables. Such a model can be cast in the form of

a linearized discrete time-invariant plant

$$(P)\begin{cases} x_p^+ = A_p x_p + B_{pu}u + B_{pw}w, \\ y = C_{py}x_p + D_{p,yu}u + D_{p,yw}w, \\ z = C_{pz}x_p + D_{p,zu}u + D_{p,zw}w, \end{cases} \tag{11}$$

where the state-space matrices are block-diagonal with n blocks, $x_p \in \mathbb{R}^{n_p}$ is the plant state, $y \in \mathbb{R}^{n_y}$ is the measurable plant output, $z \in \mathbb{R}^{n_z}$ is the performance output. The plant input $u \in \mathbb{R}^n$ is the mixing of actual plant input f_u through a non singular matrix F (see equation (8)). Similarly, considering the linearized form of the cascaded controller in equation (2), the discrete state-space form is given by

$$(C)\begin{cases} x_c^+ = A_c x_c + B_{c,y}y + B_{c,w}w + v_x, \\ y_c = C_c x_c + D_{c,y}y + D_{c,w}w + v_y, \end{cases} \tag{12}$$

where again the state-space matrices are composed of n subsystems, $x_c \in \mathbb{R}^{n_c}$ is the state of the controller, $y_c \in \mathbb{R}^n$ is the corresponding controller output, $w \in \mathbb{R}^{n_w}$ is the set-point, and $v_x \in \mathbb{R}^{n_c}$, $v_y \in \mathbb{R}^n$ are additional inputs for the AW augmentation. Assuming y_c is unbounded and leveraging the invertibility of F, interconnecting (P) and (C) through $u = y_c$ yields an *unconstrained* closed-loop system that is well-posed and internally stable. For the fixed-tilt UAV, the plant output $y = \left[\Delta x^\top \ \Delta\Theta^\top \ \Delta v^\top \ \Delta\omega^\top\right]^\top$ represents position, attitude, and their respective derivatives. The reference signal w, of the same dimension, guides tracking of the desired trajectory. However, the actual control output $y_c = f_u^d = F^{-1}w_c^d$ as illustrated in Figure 3 is inherently limited within $[\underline{u}_i, \bar{u}_i]$. Hence, the interconnection of (P) and (C) expressed by

$$f_u^a = \mathrm{sat}_{\underline{u}}^{\bar{u}}\left(F^{-1}w_c^d\right), \quad v_x = v_y = 0 \tag{13}$$

represents *constrained* or *saturated* closed-loop system where $\underline{u}_i$ and $\bar{u}_i$ denote the minimum and maximum propulsive forces the i-th actuator can generate. Whenever F is not diagonal, the closed loop loses its decentralized structure during saturation. To alleviate this effect, the compensation signals v_x, v_y are injected in equation (12); these signals are the outputs of the linear filter

$$(AW)\begin{cases} x_{aw}^+ = B_{aw}dq \\ \begin{bmatrix} v_x \\ v_y \end{bmatrix} = \begin{bmatrix} 0 \\ I_{n_u} \end{bmatrix} x_{aw} + \underbrace{\begin{bmatrix} \bar{D}_{aw} \\ 0_{n_u} \end{bmatrix}}_{D_{aw}} dq, \end{cases} \tag{14}$$

such that

$$dq = F^{-1}w_c^d - \mathrm{sat}_{\underline{u}}^{\bar{u}}\left(F^{-1}w_c^d\right), \tag{15}$$

where $x_{aw} \in \mathbb{R}^{n_{aw}}$ is the AW state and $dq \in \mathbb{R}^n$ is the input to the AW compensator. The AW compensator in equation (14) corresponds to a static full-authority AW in which the signal v_y is cascaded with a unit delay, which is included to avoid the algebraic loop otherwise arising in the controller [15]. The interconnection of (11), (12) and (14) through dq can be written in compact form by introducing the augmented closed-loop (ACL) given by

$$(ACL)\begin{cases} x_a^+ = A_a x_a + B_{a,q}dq + B_{a,w}w, \\ z = C_{a,z}x_a + D_{a,zq}dq + D_{a,zw}w, \\ y_c = C_{a,u}x_a + D_{a,uq}dq + D_{a,uw}w, \end{cases} \tag{16}$$

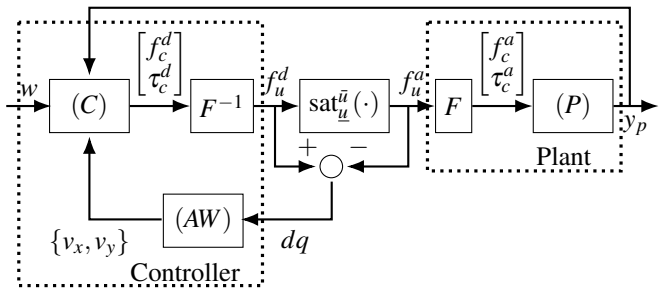

Fig. 3. Anti-Windup Augmentation Scheme

where $x_a = (x_p,\, x_c,\, x_{aw})$. In contrast to the majority of works in the framework of DLAW design [14], which are focused on the minimization of the ℓ_2-gain from w to z, we propose a discrete-time version of the performance-oriented approach developed for continuous-time systems in [9]. Such an approach starts by defining a reference model (RM)

$$(RM)\begin{cases} x_{rm}^+ = A_{rm}x_{rm} + B_{rm,w}w, \\ z_{rm} = C_{rm,z}x_{rm} + D_{rm,zw}w, \end{cases} \tag{17}$$

which is used to describe the (desired) unconstrained closed-loop behavior. As conditions inducing propeller saturation can be assimilated with the use of step references, we include the filter

$$(FL) \quad w^+ = I_{n_w}(1-\varepsilon)w, \quad w(0) = w_0, \quad \mathbb{R}_{>0} \ni \varepsilon \ll 1, \tag{18}$$

into the closed-loop system used for the AW synthesis, as suggested in [9] to achieve good time-domain responses in practical conditions (the initial condition of the filter w_0 can be considered as the step amplitude). Thus, by defining the augmented state $\xi = [x_a^\top \ x_{rm}^\top \ w^\top]^\top \in R^{n_\xi}$, the interconnection of equations (16), (17) and (18) through dq is given compactly by

$$\begin{cases} \xi^+ = A\xi + B_q dq, \\ z_e = C_z\xi + D_{zq}dq, \\ y_c = C_y\xi + D_{yq}dq, \end{cases} \tag{19}$$

where all the involved matrices can be uniquely determined from equations (11), (12), (14), (17) and (18) and where $z_e = z - z_{rm}$ is a performance output introduced to evaluate the mismatch between the reference and the actual system response. Starting from the above representation, the problem that we will address can be formulated as follows.

Problem 1: Given the compact representation in equation (19), find the matrices of the AW compensator as defined in equation (14) such that the ℓ_2-norm of the performance output z_e is as small as possible.

The solution to *Problem 1* can be carried out by exploiting an extension of the well-known generalized sector condition (see, e.g., [14]).

Lemma 1: Consider any diagonal matrix $M \in \mathbb{R}^{n\times n}$, $H \in \mathbb{R}^{n\times n_\xi}$, a non-singular matrix $F \in \mathbb{R}^{n\times n}$. Then, the following condition holds

$$-dq^T M(dq - y_c + H\xi) \geq 0, \quad \forall \xi \in \mathbb{R}^{n_\xi} : \ \mathrm{sat}(H\xi) = H\xi. \tag{20}$$

The synthesis of the anti-windup (AW) compensation matrices can be performed following the procedure described

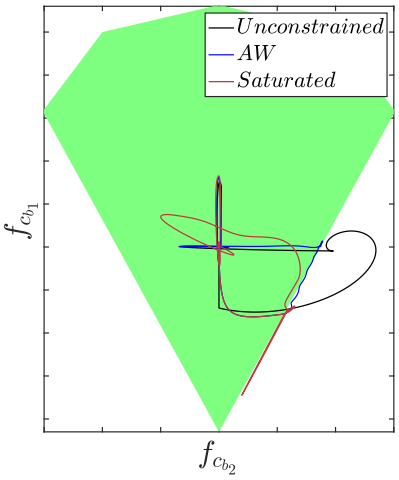

Fig. 4. Applied lateral and longitudinal forces on the fixed-tilt UAV by different controllers (scale not shown for confidentiality)

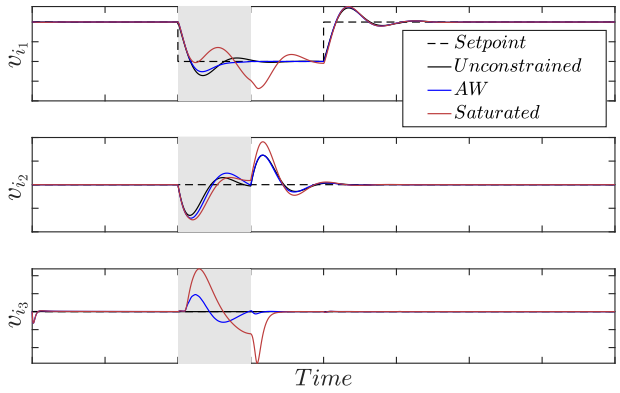

Fig. 5. Velocity tracking performance for fixed-tilt UAV using various controllers (scale not shown for confidentiality)

in [7] and is therefore omitted here. The method relies on the definition of a set of n_r directions of interest, denoted as $w_{0_1}, \ldots, w_{0_{n_r}} \in \mathbb{R}^{n_w}$, and the selection of a diagonal weighting matrix $W \in \mathbb{R}^{n \times n}$, which is used to prioritize the control objectives. The considered synthesis procedure ensures that the ellipsoid $\mathcal{E}\left(Q^{-1}\right) = \{\xi \in \mathbb{R}^{n_\xi} : \xi^\top Q^{-1} \xi < 1\}$ is contained in the region of attraction of (19) and $\overline{\text{co}}\left((0, w_{0_h}) \in \mathbb{R}^{n_\xi}, h = 1, \ldots, n_r\right) \subset \mathcal{E}(Q^{-1})$, for some $Q = Q^\top$ positive definite. Moreover, the following condition on the ℓ_2 norm of z_e is satisfied

$$\sum_{t=0}^{\infty} z_e^\top W^2 z_e \leq \gamma, \quad \forall \xi(0) \in \mathcal{E}(Q^{-1}). \tag{21}$$

The main idea behind the considered design method consists in first selecting reasonable step amplitudes by defining the vectors r_i and then tuning the AW compensator in such a way that the *unconstrained* response is tracked at best for the given references. Since minimizing γ leads to a lower weighted mismatch z_e, this objective can be achieved by solving a semi-definite program (see [7] for details).

V. Simulation Results

This section demonstrates the capability of the proposed AW compensation method in addressing saturation issues in fixed-tilt UAVs. The AW synthesis is carried out using an overall plant model that integrates the linearized dynamics of the UAV (see equation 10) with the *input* matrix. In parallel, the baseline controller is extended by incorporating the *mixer* matrix as depicted in Figure 3. The AW compensator, as introduced in (14), is augmented with the controller states and outputs with v_x and v_y respectively. As discussed in Section IV, the synthesis procedure is applied to a specific reference system. In our implementation, the AW gain is optimized using step references for velocity, position, angular velocity, and attitude, defined as

$$w_0 = \begin{bmatrix} w_{0,\Delta v}^\top & w_{0,\Delta p}^\top & w_{0,\Delta \omega}^\top & w_{0,\Delta \Theta}^\top \end{bmatrix}^\top, \tag{22}$$

where w_0 represents the amplitude of the step references as an input to the filter (FL) as given in equation (18). The step reference amplitudes were carefully selected to independently excite the platform's translational and rotational dynamics. This is critical, as it facilitates the design of AW gains that effectively account for saturation during full actuation. Following numerical testing of the synthesis algorithm, the AW gains are obtained via LMI optimization for the following set of step reference magnitudes

$$w_0 = \begin{cases} \begin{bmatrix} w_{0,\Delta v}^\top & \vec{0} & \vec{0} & \vec{0} \end{bmatrix}^\top, \\ \begin{bmatrix} \vec{0} & w_{0,\Delta p}^\top & \vec{0} & \vec{0} \end{bmatrix}^\top, \\ \begin{bmatrix} \vec{0} & \vec{0} & w_{0,\Delta \omega}^\top & \vec{0} \end{bmatrix}^\top, \\ \begin{bmatrix} \vec{0} & \vec{0} & \vec{0} & w_{0,\Delta \Theta}^\top \end{bmatrix}^\top, \end{cases} \tag{23}$$

where $w_{0,\Delta v} = [\pm 2,\ \pm 2,\ 0]^\top$m/s, $w_{0,\Delta p} = [\pm 5,\ \pm 5,\ 3]^\top$m, $w_{0,\Delta \omega} = [\pm 50,\ \pm 50,\ \pm 90]^\top$deg/s, $w_{0,\Delta \Theta} = [\pm 10,\ \pm 10,\ \pm 180]^\top$deg , and $\vec{0}$ is the zero vector in $\mathbb{R}^{1\times 3}$.

Simulation results are presented for a reference trajectory that utilizes the platform's full actuation, resembling the scenario of aerial interaction under wind gusts. A step reference velocity of 1 m/s along the longitudinal (b_1) axis is imposed, with a corresponding negative position reference ensuring that the longitudinal forces fall within the narrow lower portion of the force envelope (see Figure 2). Simultaneously, a steady external force is applied along the lateral (b_2) axis, saturating the platform; this simulates a maneuver along b_1 with a steady attitude under a wind gust along b_2. As shown in Figure 4, the set-points force the unconstrained controller to demand forces beyond the envelope, while both the saturated and AW-compensated controllers remain within bounds. Moreover, the saturated controller exhibits prolonged windup compared to the AW solution, increasing the risk of recovery failure. Figure 5 compares set-point tracking performance, revealing that saturation induces transient dynamics—such as cross-coupling and vertical overshoot—that may lead to altitude loss. The shaded area in Figure 5 indicates that an external force is applied along b_2.

Figure 6 and Figure 7 show the position and attitude reference tracking by different controllers. Notably, the AW-augmented controller closely follows the unconstrained controller's performance, even though the applied forces differ significantly (see Figure 4). Additionally, the saturated controller exhibits transient dynamics that can lead to altitude loss when pitch and roll exceed 10°. In contrast, the

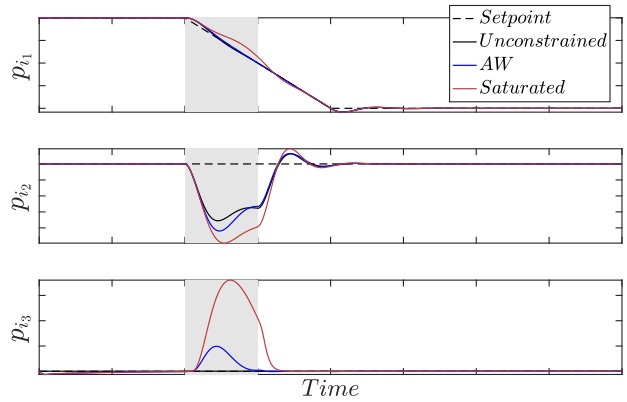

Fig. 6. Position tracking performance for fixed-tilt UAV using various controllers (scale not shown for confidentiality)

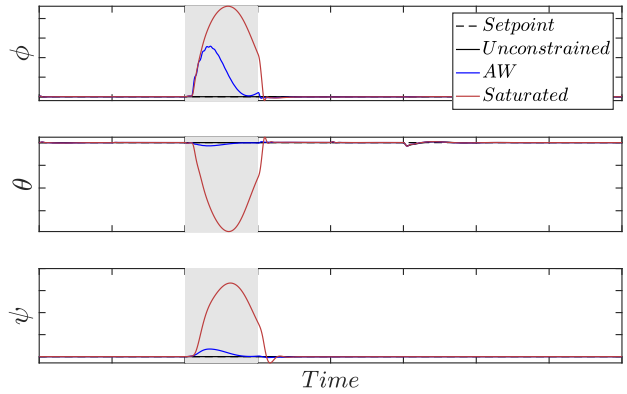

Fig. 7. Attitude tracking performance for fixed-tilt UAV using various controllers (scale not shown for confidentiality)

AW-augmented controller maintains stability and minimizes performance degradation during saturation. Figure 8 shows the applied propeller forces. The second propeller saturates at the lower limit, causing the baseline controller to deviate sharply from the unconstrained case, while the anti-windup controller remains close to the desired behavior.

VI. Conclusions

This paper presents an effective anti-windup compensation method to address saturation effects in fixed-tilt UAVs. By integrating linearized dynamics with allocation and mixer matrices, our approach enables robust full actuation under severe saturation. Simulation results show that the AW-augmented controller approximates the unconstrained controller's performance while reducing adverse transient behavior seen with conventional saturation. Our analysis also highlights the direction-dependent force limits imposed by the tiltrotor configuration, ultimately enhancing UAV performance during complex maneuvers. Future work will focus on experimental validation.

VII. Acknowledgement

This work is supported by the European Union – NextGenerationEU under the National Recovery and Resilience Plan (PNRR), Mission 4, Component 2 "From Research to Enterprise" – Investment 3.3, within the framework of the doctorate program activated under Ministerial Decree No. 352 of 9/04/2022.

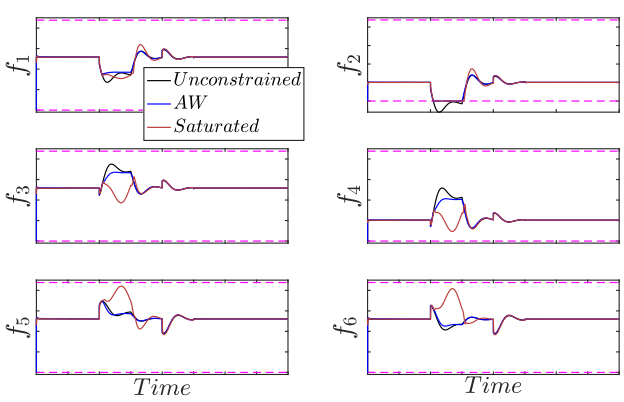

Fig. 8. Applied propeller forces for fixed-tilt UAV using various controllers (scale not shown for confidentiality)

References

[1] A. Ollero, M. Tognon, A. Suarez, D. Lee, and A. Franchi, "Past, Present, and Future of Aerial Robotic Manipulators," *IEEE Transactions on Robotics*, vol. 38, no. 1, pp. 626–645, 2 2022.

[2] F. Ruggiero, V. Lippiello, and A. Ollero, "Aerial Manipulation: A Literature Review," *IEEE Robotics and Automation Letters*, vol. 3, no. 3, pp. 1957–1964, 7 2018.

[3] D. Mayne, J. Rawlings, C. Rao, and P. Scokaert, "Constrained model predictive control: Stability and optimality," *Automatica*, vol. 36, no. 6, pp. 789–814, 6 2000.

[4] K. Shao, J. Zheng, R. Tang, X. Li, Z. Man, and B. Liang, "Barrier Function Based Adaptive Sliding Mode Control for Uncertain Systems With Input Saturation," *IEEE/ASME Transactions on Mechatronics*, vol. 27, no. 6, pp. 4258–4268, 12 2022.

[5] L. Zaccarian and A. R. Teel, *Modern Anti-windup Synthesis: Control Augmentation for Actuator Saturation*. Princeton University Press, 2011. [Online]. Available: http://ieeexplore.ieee.org/document/9452439

[6] N. Buratti, D. Invernizzi, and M. Lovera, "Experimental validation of LMI-based anti-windup compensators for attitude control in multirotor UAVs," *IFAC-PapersOnLine*, vol. 52, no. 12, pp. 164–169, 2019.

[7] P. Ghignoni, N. Buratti, D. Invernizzi, and M. Lovera, "Anti-windup design for directionality compensation with application to quadrotor UAVs," *IEEE Control Systems Letters*, pp. 1–1, 2020.

[8] J. G. Da Silva and S. Tarbouriech, "Antiwindup design with guaranteed regions of stability: an LMI-based approach," *IEEE Transactions on Automatic Control*, vol. 50, no. 1, pp. 106–111, 1 2005.

[9] J.-M. Biannic and S. Tarbouriech, "Optimization and implementation of dynamic anti-windup compensators with multiple saturations in flight control systems," *Control Engineering Practice*, vol. 17, no. 6, pp. 703–713, 6 2009.

[10] "ARIES: A Flying Robot Platform for NDT Contact Inspections," https://antx.it/industrial-drones-antx/aries/, accessed: [05/02/2025].

[11] N. Staub, D. Bicego, Q. Sable, V. Arellano, S. Mishra, and A. Franchi, "Towards a Flying Assistant Paradigm: the OTHex," in *2018 IEEE International Conference on Robotics and Automation (ICRA)*. IEEE, 5 2018, pp. 6997–7002.

[12] D. Invernizzi, M. Giurato, P. Gattazzo, and M. Lovera, "Full Pose Tracking for a Tilt-Arm Quadrotor UAV," in *2018 IEEE Conference on Control Technology and Applications (CCTA)*. IEEE, 8 2018, pp. 159–164.

[13] M. Perin, M. Bertoni, N. Viezzer, G. Michieletto, and A. Cenedese, "Star-shaped Tilted Hexarotor Maneuverability: Analysis of the Role of the Tilt Cant Angles," in *2024 IEEE 20th International Conference on Automation Science and Engineering (CASE)*. IEEE, 8 2024, pp. 1791–1797.

[14] S. Galeani, S. Tarbouriech, M. Turner, and L. Zaccarian, "A Tutorial on Modern Anti-windup Design," *European Journal of Control*, vol. 15, no. 3-4, pp. 418–440, 1 2009.

[15] A. Syaichu-Rohman and R. H. Middleton, "Anti-windup schemes for discrete time systems: an LMI-based design," in *2004 5th Asian Control Conference (IEEE Cat. No.04EX904)*, vol. 1, 2004, pp. 554–561.